Article

Immunity

Regulatory T Cells in Tumor-Associated Tertiary Lymphoid Structures Suppress Anti-tumor T Cell Responses

Graphical Abstract

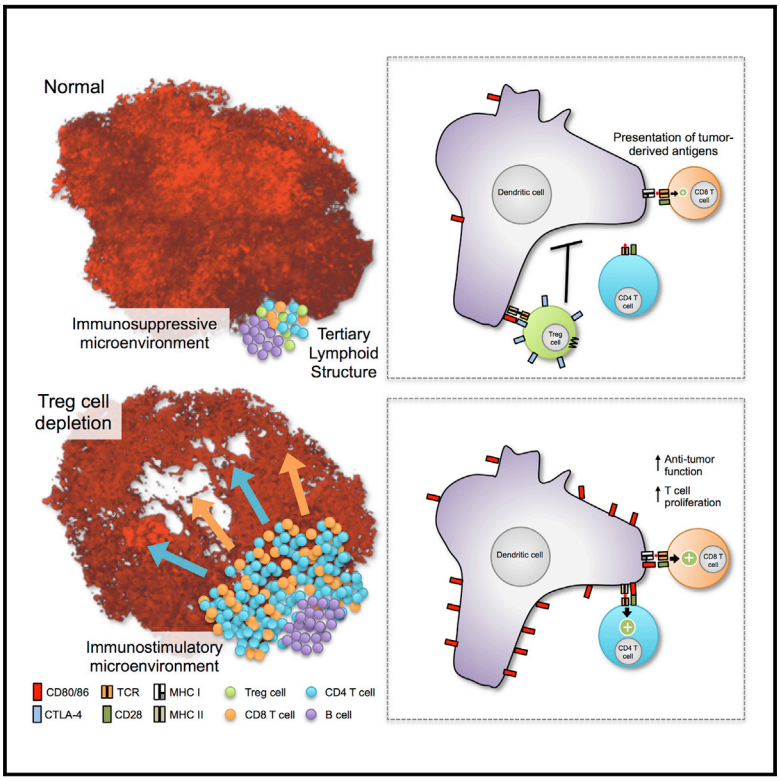

Highlights

- TA-TLSs form adjacent to advanced lung tumors
- TA-TLSs have features and functions of lymph nodes
- Treg cells in TA-TLSs actively suppress immune responses
- Therapeutic Treg cell depletion causes immune-mediated tumor destruction

Authors

Nikhil S. Joshi, Elliot H. Akama-Garren, Yisi Lu, ..., Denise M. Crowley, Roderick T. Bronson, Tyler Jacks

Correspondence

tjacks@mit.edu

In Brief

Intratumoral regulatory T (Treg) cells are important in lung cancer, but it has been difficult to dissect their mechanisms of action. Jacks and colleagues demonstrate that intratumoral Treg cells function within tumor-associated tertiary lymphoid structures to suppress anti-tumor T cell responses in a mouse model of lung cancer.

Joshi et al., 2015, Immunity *43*, 579–590
September 15, 2015
http://dx.doi.org/10.1016/j.immuni.2015.08.006

CellPress

Immunity
Article

Regulatory T Cells in Tumor-Associated Tertiary Lymphoid Structures Suppress Anti-tumor T Cell Responses

Nikhil S. Joshi,[1] Elliot H. Akama-Garren,[1] Yisi Lu,[1] Da-Yae Lee,[1] Gregory P. Chang,[1] Amy Li,[1] Michel DuPage,[1] Tuomas Tammela,[1] Natanya R. Kerper,[1] Anna F. Farago,[1] Rebecca Robbins,[1] Denise M. Crowley,[1] Roderick T. Bronson,[3] and Tyler Jacks[1,2,*]

[1]Koch Institute for Integrative Cancer Research and Department of Biology, Massachusetts Institute of Technology, Cambridge, MA 02142, USA
[2]Howard Hughes Medical Institute, Massachusetts Institute of Technology, Cambridge, MA 02142, USA
[3]Department of Pathology, Tufts University School of Medicine and Veterinary Medicine, North Grafton, MA 01536, USA
*Correspondence: tjacks@mit.edu
http://dx.doi.org/10.1016/j.immuni.2015.08.006

SUMMARY

Infiltration of regulatory T (Treg) cells into many tumor types correlates with poor patient prognoses. However, mechanisms of intratumoral Treg cell function remain to be elucidated. We investigated Treg cell function in a genetically engineered mouse model of lung adenocarcinoma and found that Treg cells suppressed anti-tumor responses in tumor-associated tertiary lymphoid structures (TA-TLSs). TA-TLSs have been described in human lung cancers, but their function remains to be determined. TLSs in this model were spatially associated with >90% of tumors and facilitated interactions between T cells and tumor-antigen-presenting dendritic cells (DCs). Costimulatory ligand expression by DCs and T cell proliferation rates increased in TA-TLSs upon Treg cell depletion, leading to tumor destruction. Thus, we propose that Treg cells in TA-TLSs can inhibit endogenous immune responses against tumors, and targeting these cells might provide therapeutic benefit for cancer patients.

INTRODUCTION

Non-small-cell lung cancer (NSCLC), including lung adenocarcinoma, accounts for ~25% of all cancer deaths (Jemal et al., 2010), and despite improvements in therapy, NSCLC mortality remains around 80% (http://seer.cancer.gov/statfacts/html/lungb.html). Immunotherapy uses the immune system to attack cancer and has demonstrated durable tumor regression in "immunogenic" tumor types such as melanoma (Pardoll, 2012). Yet, until recently, NSCLC was considered "non-immunogenic" because tumors responded poorly to immunotherapeutics (Raez et al., 2005). Furthermore, it was thought that compared to melanomas, lung tumors might not elicit strong endogenous T cell responses, even though these tumor types had similar numbers of mutations and predicted neoantigens (Rajasagi et al., 2014; Vogelstein et al., 2013). The recent success of immune-checkpoint inhibitors in NSCLC patients demonstrates that anti-tumor T cell responses do exist in a significant fraction of lung cancer patients, but they are functionally inhibited by poorly understood immunosuppressive mechanisms (Pardoll, 2012). Overcoming these mechanisms will be essential for generating more-effective immunotherapies for this disease.

Regulatory T cell (Treg) deficiency, through mutation or deletion of X-linked forkhead box P3 (*Foxp3*), leads to a fatal lymphoproliferative disease (Josefowicz et al., 2012). However, Treg cells might also facilitate tumor progression by suppressing adaptive immunity against tumors. Treg cell depletion in transplantable, carcinogen-induced, and autochthonous tumor models demonstrates increased anti-tumor immune responses, even against previously established tumors, which results in reductions in tumor size (Sakaguchi, 2004; Bos et al., 2013; Teng et al., 2010). Yet, many questions remain about how and where Treg cells function in the context of developing tumors.

Treg cells suppress self-reactive T cells in secondary lymphoid organs (SLOs; e.g., lymph nodes [LNs] and spleen). Similarly, Treg cells can suppress anti-tumor responses in tumor-draining LNs (Boissonnas et al., 2010; Campbell and Koch, 2011). However, Treg cells inside tumor tissues might also be important in natural tumor progression. Treg cells are often enriched in tumor tissue, and a high ratio of intratumoral Treg cells to effector T cells generally predicts poor patient outcomes (Fridman et al., 2012). Furthermore, the ability of anti-CTLA-4 antibodies to deplete intratumoral, but not LN, Treg cells is critical for their efficacy in animal cancer models (Marabelle et al., 2013; Selby et al., 2013; Simpson et al., 2013). However, although previous data have suggested that intratumoral Treg cells promote tumor development, the mechanisms by which they do so remain to be fully determined.

In patients, across cancer types, lymphocytes can be found in LN-like, large, complex tumor-associated tertiary lymphoid structures (TA-TLSs; Fridman et al., 2012; Goc et al., 2013). Among patients with early-stage NSCLC, ~70% have TA-TLSs, which contain immune cells with an activated phenotype, as do TLSs observed after viral infection (Neyt et al., 2012; de

Chaisemartin et al., 2011; Dieu-Nosjean et al., 2008). TA-TLS presence also correlates with increased overall survival. Thus, it is thought that TA-TLSs promote anti-tumor responses. However, TA-TLSs have not been described in animal models, and their proposed functions have not been experimentally tested. It is also uncertain whether immunosuppressive pathways are active in TA-TLSs.

Genetically engineered mouse models (GEMMs) of cancer have greatly informed the understanding of tumor biology and therapy (Hayes et al., 2014; Kwon and Berns, 2013). Tumors in GEMMs develop from untransformed cells in their native microenvironment and, importantly, in the presence of a fully functional immune system. However, tumors in GEMMs are often poorly immunogenic, and consequentially, the use of GEMMs for tumor immunology studies has lagged (DuPage and Jacks, 2013). We previously programmed autochthonous sarcomas and lung adenocarcinomas in "KP" (*Kras*$^{\text{Lox-STOP-Lox(LSL)-G12D}}$*Trp53*$^{\text{flox/flox}}$) mice to express "LucOS," firefly luciferase fused to a portion of ovalbumin (ova, encoding the potent T cell OT-I and OT-II antigens) and the antigenic 2C peptide (DuPage et al., 2011; DuPage et al., 2012). In both tumor types, tumor-specific T cells had a significant impact on tumor development, but disease outcomes differed. T cells prevented the development of LucOS-expressing sarcomas and, consequentially, only "edited" (LucOS-negative) sarcomas developed (DuPage et al., 2012). In contrast, although T cells restrained the growth of LucOS-expressing lung tumors early in the disease course, they could not prevent it (DuPage et al., 2011). Moreover, this initial impact on tumor growth was followed by immune suppression, despite the confirmed expression of LucOS by tumors. Therefore, whereas sarcomas escaped immune control via editing, lung tumors escaped because the anti-tumor response itself was suppressed. The mediators of immunosuppression in the lung adenocarcinoma model are unknown. Because Treg cells are prominent in early LucOS-expressing tumors (DuPage et al., 2011), we reasoned that they might be important in immune suppression in later-stage tumors. Here, we investigated the functions of intratumoral Treg cells in advanced lung adenocarcinomas.

RESULTS

Treg Cells Accumulate in Tumor-Bearing Lungs and Have an Activated Phenotype

To identify and deplete Treg cells in autochthonous lung tumors, we bred KP mice to *Foxp3*$^{\text{IRES-DTR-GFP}}$ mice (Kim et al., 2007), in which all CD4$^+$FoxP3$^+$ Treg cells express diphtheria toxin receptor (DTR)-GFP fusion protein. Lung tumors in "KP-F" mice (F: *FoxP3*$^{\text{DTR-GFP/DTR-GFP}}$ or *KP-FoxP3*$^{\text{DTR-GFP/y}}$) were initiated by intratracheal (i.t.) administration of non-replicating lentiviruses co-expressing LucOS and Cre-recombinase (LucOS/Cre LV; DuPage et al., 2011). In lung epithelial cells, Cre activates oncogenic *Kras*$^{\text{G12D}}$ and deletes *Trp53*, resulting in the development of autochthonous lung adenocarcinomas over a period of months (Figure S1A; DuPage et al., 2011). After 20–24 weeks, KP-F mice had a mixture of low- and high-grade lung adenocarcinomas with few infiltrating lymphocytes (Figure S1B).

To identify circulating and lung-tissue Treg cells in flow cytometric analysis, we labeled the circulating cells with anti-CD45 (CD45$^{\text{PE-CF594}}$) antibodies injected prior to sacrifice (Figure S1C). In control week-20 LucOS-infected P-F (*Kras*$^{+/+}$) mice, most "lung" CD4$^+$ T cells or Treg cells were in the circulation (CD45$^{\text{PE-CF594+}}$), but in tumor-bearing animals, a large fraction of the CD4$^+$ T cells and Treg cells were in the lung tissue (CD45$^{\text{PE-CF594}-}$; Figure 1A). This corresponded with a >20-fold increase in lung-tissue Treg cell numbers, whereas circulating Treg cell numbers remained unchanged (Figure 1B). Similar results were seen with excised tumors (data not shown).

Immunophenotyping demonstrated that ~60%–80% of the lung-tissue Treg cells in tumor-bearing mice expressed CD103 (integrin αE; Figure 1C), a Treg cell marker found in sites of inflammation (Feuerer et al., 2010; Sather et al., 2007; Suffia et al., 2005). Furthermore, ~50% of the CD103$^+$ Treg cells also expressed killer cell lectin-like receptor G1 (KLRG1), which is typically associated with terminally differentiated immune cells (Beyersdorf et al., 2007; Cheng et al., 2012; Joshi et al., 2007; Robbins et al., 2005). In contrast, the presence of tumors did not affect CD103 and KLRG1 expression by Treg cells in the lung circulation, tumor-draining mediastinal LN (mLN), or control inguinal LNs (iLNs; Figure 1C). CD103$^+$KLRG1$^+$ double-positive (DP) Treg cells expressed high amounts of several additional molecules previously associated with activated Treg cells, including two markers of T cell activation, CD44 and CD69, and the ectonucleotidase CD39 (Figure 1D). DP Treg cells also expressed high amounts of the interleukin-2 (IL-2) high-affinity receptor IL-2Rα (CD25), as well as the immunoinhibitory receptor PD-1 (Figure 1D). The expression of these markers by DP Treg cells was higher than that of CD103$^+$KLRG1$^-$ single-positive (SP) or CD103$^-$KLRG1$^-$ double-negative (DN) Treg cells in the lung tissue (Figure 1D). Treg cells in lung tissue also expressed higher amounts of CTLA-4 than did Treg cells in the mLN (Figure 1E). Together, these data suggest that similar to Treg cells found at sites of inflammation, tumor-infiltrating Treg cells exhibit an activated phenotype. Because few Treg cells with this phenotype were observed in the draining LN, it is likely that Treg cells acquired their activated phenotype within the tumor-bearing lung.

Treg Cells Actively Suppress Anti-tumor Responses Targeting Established Lung Adenocarcinomas

We next assessed the effect of Treg cell depletion on tumors in KP-F mice. Two intraperitoneal (i.p.) injections of diphtheria toxin (DT, 50 μg/g) into tumor-bearing (~18–20 weeks after infection) or non-tumor-bearing KP-F mice efficiently eliminated Treg cells in the lungs and lymphoid tissues (Figures 2A, S2A, and S2B). However, *FoxP3*$^{\text{DTR}}$ mice, but not *FoxP3*$^{\text{WT}}$ mice, became moribund within ~2–3 weeks of depletion and required sacrifice (Figure S2C). Additionally, in tumor-bearing KP-*Foxp3*$^{\text{DTR}-\text{GFP/+}}$ (KP-F/+) mice, in which only 50% of all Treg cells express DTR-GFP as a result of X inactivation (Figure S2D), DT treatment did not cause morbidity (data not shown). Therefore, the observed morbidity was caused by an autoimmune response triggered by transient Treg cell depletion and was not a side effect of DT treatment. Consistent with this, 12 days after depletion, in KP-F mice, but not in KP-F/+ mice, most T cells were activated (CD44$^{\text{hi}}$), there was dramatic lymphadenopathy and splenomegaly, and lymphocytes had infiltrated several tissues throughout the body (Figures S2E–S2H; Kim et al., 2007). Of note, regardless of tumor status, in Treg-cell-depleted mice we

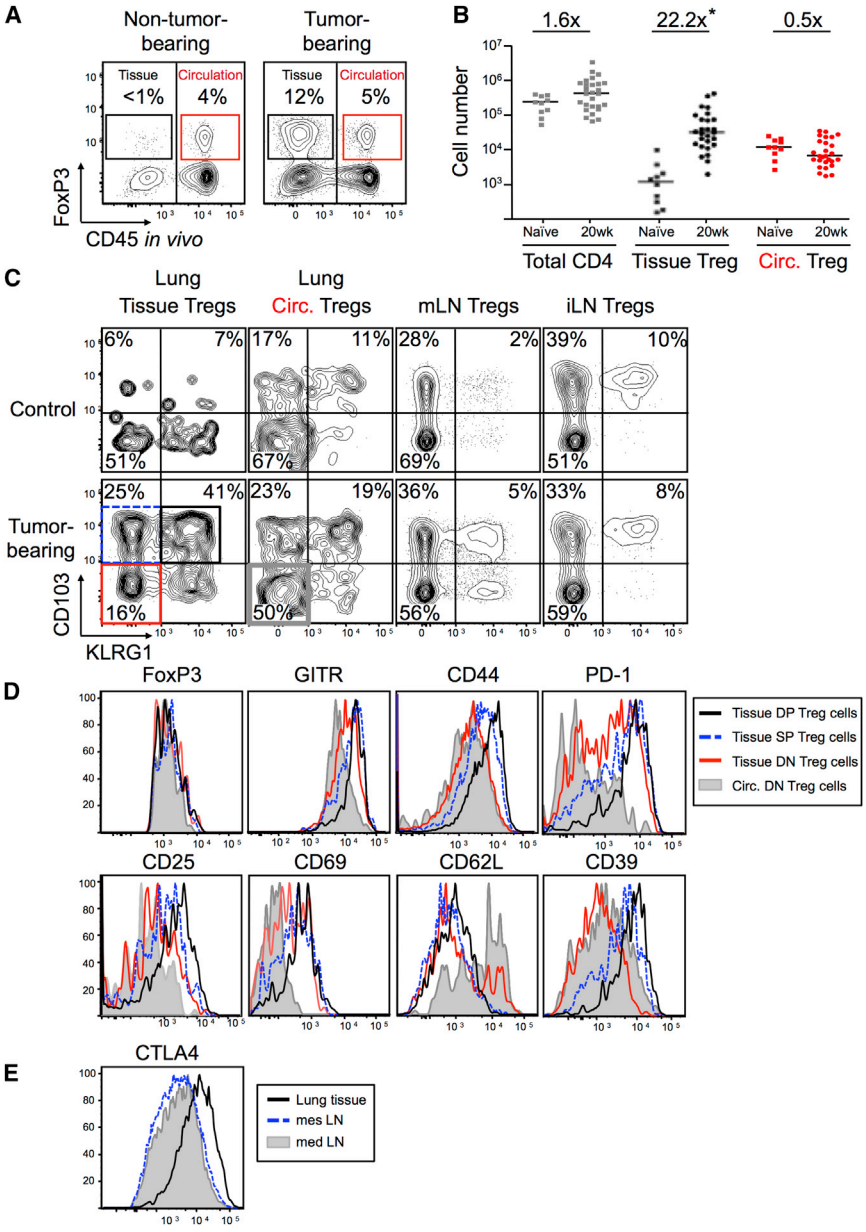

Figure 1. Treg Cells in Tumor-Bearing Lungs Have an Activated Phenotype

KP-F and P-F (control) mice were analyzed ~20 weeks (18–24 weeks) after LucOS/Cre LV infection by flow cytometry.

(A) FACS plots gated on lung CD4$^+$ T cells. Tissue (black) and circulating (red) FoxP3$^+$ Treg cell frequency is indicated. Note that control and uninfected (naive) lungs were indistinguishable. n > 30 mice.

(B) Graph of total CD4$^+$ T cells and tissue and circulating Treg cell numbers in lungs from naive (n = 11) and tumor-bearing (week 20, n = 30) animals. Median and relative differences are indicated. *p = 0.03.

(C) CD103 and KLRG1 on the Treg cell populations in (A). n > 30 mice.

(D) Expression of indicated markers by circulating DN (filled gray line) and tissue DN, SP, and DP Treg cells (red, dashed blue, and black lines, respectively). Histograms are gated as shown in (C). n = 9–35 mice.

(E) CTLA-4 expression by mLN (gray filled line), mesenteric (mes) LN (dashed blue line), and lung-tissue Treg cells (black line). n = 7 mice.

observed lymphocytic infiltration near the major airways in the lungs and goblet cell metaplasia, similar to what is seen in FoxP3-deficient mice (Figures S2I and S2J; Lin et al., 2005). However, in non-tumor-bearing animals, the alveolar spaces in the lungs (where tumors normally develop) were free from infiltration.

To track tumor cell fate after Treg cell depletion, we bred KP-F mice to *Rosa26*$^{LSL\text{-}tdTomato(tdT)}$ mice to generate "KPT-F" mice, in which Cre induces tdT expression in tumor cells (Figure S1A; Madisen et al., 2010). Immunofluorescence (IF) staining of tumors from untreated ~week-20 KPT-F mice demonstrated that they were composed of abundant, healthy-appearing tdT$^+$ tumor cells that were arranged primarily in papillary structures with EpCAM staining junctions between adjacent tumor cells (Figure 2B). In contrast, day-12 Treg-cell-depleted tumors had a range of cellular infiltration and disruption of regular tissue architecture (Figure 2B). Quantification of 85 control and 108 Treg-cell-depleted tumors showed that >80% of the Treg-cell-depleted tumors had moderate or severe disruption (Figure 2C). To visualize tumor destruction more comprehensively, we performed CLARITY (Chung et al., 2013) on lungs from control and Treg-cell-depleted KPT-F mice. This allowed whole-tumor 3D confocal imaging of 15 control and 10 Treg-cell-depleted tumors. Tumors from the Treg-cell-depleted mice showed extensive cellular infiltration (Figure 2D and Movie S1) and contained cavities filled with densely packed (non-tumor) cells. Furthermore, tumor cells in the Treg-cell-depleted mice were thin and elongated and no longer formed connections with adjacent tumor cells (Figures 2B and 2D). These data demonstrate that the cellular density and morphology of tumors were severely disrupted by Treg cell depletion.

Immunohistochemical (IHC) analysis showed that most of the infiltrating cells in Treg-cell-depleted tumors were CD45$^+$ immune cells (Figure 2E). Infiltration was highly focused in the areas near tumors, given that distal areas were free of immune infiltrates (Figure S3A). Immune infiltration was not observed in tumors from Treg-cell-depleted KPT-F/+ mice, indicating that depletion of more than half of the Treg cell population was required for anti-tumor effects (Figure S3B). Fluorescence-activated cell sorting (FACS) analysis revealed that the number of CD4$^+$ and CD8$^+$ T cells in the lung increased after Treg cell depletion (Figure 2F). In contrast, the number of B cells did not

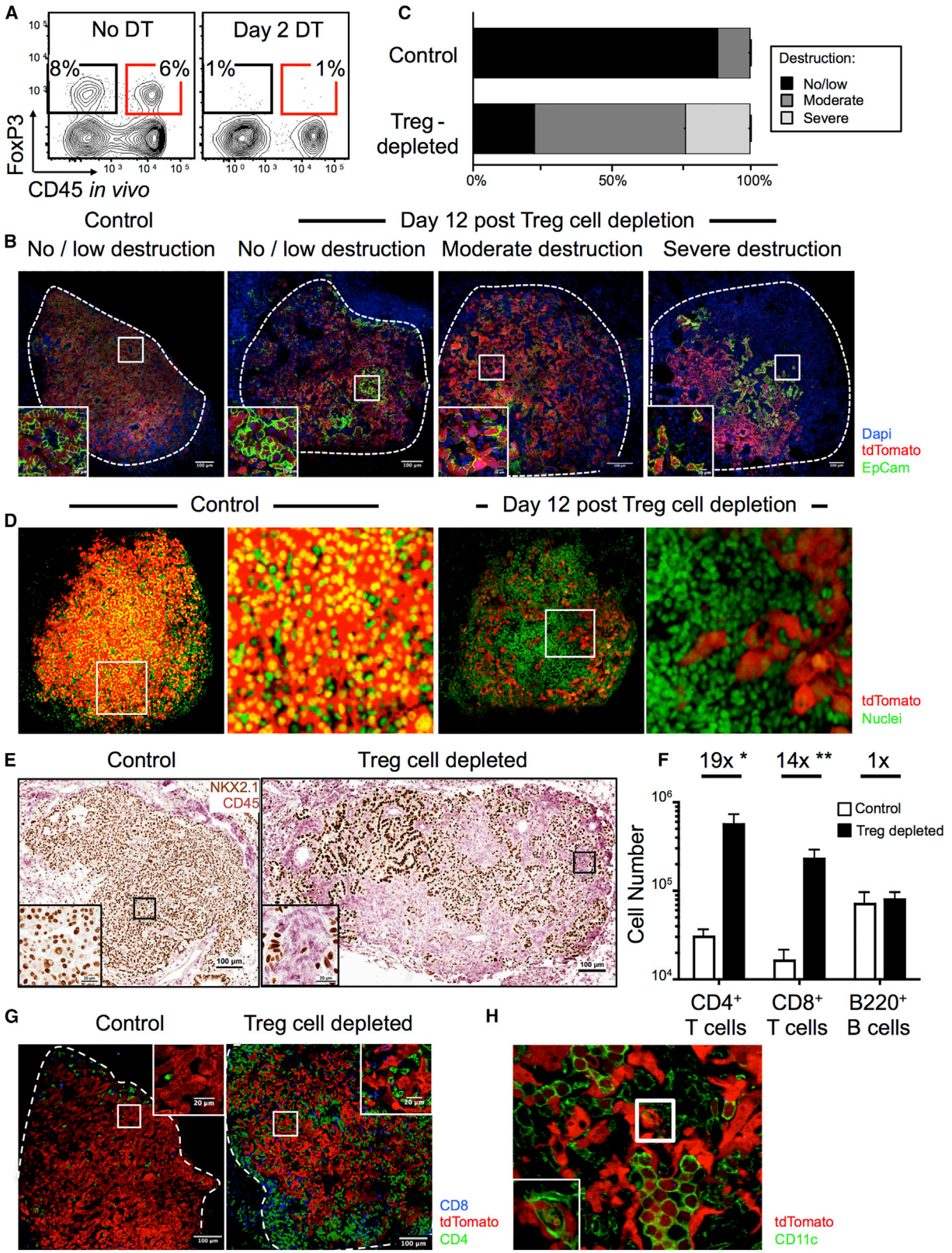

Figure 2. Treg Cells Maintain Immune Quiescence in Advanced Tumors

~Week-18 to week-20 LucOS/Cre-LV-infected KP-F (A) or KPT-F (B–H) mice were treated 1× (A) or 2× (B–H) with i.p. DT (50 ng/g) and analyzed 2 (A) or 12 (B–H) days later.

(legend continued on next page)

increase. IF analyses showed that in undepleted mice, $CD3^+$ T cells in tumors were primarily located within or near blood vessels, and $CD11c^+$ macrophages were located within airway-like pockets surrounded by tumor cells (Figures S4A and S4B). In contrast, in the absence of Treg cells, $CD4^+$ and $CD8^+$ T cells were located throughout the tumor parenchyma (Figure 2G), and tumors were heavily infiltrated by macrophages that were faintly positive for tdT (Figure 2H). Moreover, a small number of macrophages had tdT^+ vesicles, suggesting phagocytosis of tumor cells. Together, these data demonstrate that Treg cells actively suppress immune destruction of established tumors.

Lung-Tissue Treg Cells Are Contained within TA-TLSs

We next investigated Treg cell localization in tumor-bearing lungs. Tumors in week-20 KP-F mice had few infiltrating Treg cells, and instead, most Treg cells (>80-fold increase) were located in perivascular immune cell patches resembling TLSs (Figures 3A and 3B). These structures also contained $CD11c^+$ dendritic cells (DCs) and $B220^+$ B cells, two cell types that have the potential to interact directly with Treg cells (Figure 3C). TA-TLSs have been observed in patients with lung adenocarcinoma (Fridman et al., 2012), but not in animal tumor models. Therefore, we quantified the extent to which TLSs were associated with tumors in this model and identified whether they displayed features of TA-TLSs in human cancers.

Because tumors span several hundred microns, we reasoned that analyses of thin (5-μm) lung sections might underestimate the presence of TLSs in tumor-bearing lungs. Therefore, we quantified the presence of TLSs in 30-μm-thick sections of tumor-bearing lungs from eight mice and counted the number of tumors that were associated with TLSs in three in-silico-reconstructed tumor-bearing lung lobes (Figure 3D). Analysis of the 30-μm sections revealed that ~60% (18/31) of tumors were directly associated with at least one TLS (defined as B cell clusters of >10 cells directly associated with T cells), and analysis of the in-silico-reconstructed lungs showed at least one TLS associated with ~93% (70/75) of tumors analyzed (data not shown).

We next used IF to characterize the cellular and structural components of TLSs in thick sections of tumor-bearing lungs. TLSs varied greatly in size and complexity, although this might be due to the fact that individual sections only capture part of a given TLS. TA-TLSs in human cancers can have B and T cell zones organized by follicular dendritic cells (FDCs) and fibroblastic reticular cells (FRCs). Similarly, in this model, mature TLSs had clearly defined $B220^+$ B cell and $CD3^+$ T cell areas, which were distinct from the $NKX2.1^+$ tumor areas (Figures 3E–3I). Moreover, TLSs all contained Treg cells, which were primarily located in the T cell areas (Figure 3E-II). About 30% of the time, B cell areas in the TLSs contained detectable $CR1^+$ cells with long processes that were morphologically similar to FDCs (Figure 3E-III). These cells also expressed the B cell chemoattractant CXCL13 and made direct contact with B cells (Figure 3E-III and Movie S2A). We also observed that many T cells in the T cell areas were in direct contact with $ERTR\text{-}7^+CCL21^+$ FRC-like cells (Figure 3E-IV and Movie S2B). The presence of FRC- and FDC-like cells in TA-TLSs suggests that they could help to organize and support infiltrating B and T cells.

Human TA-TLSs contain high endothelial venules (HEVs), which in LNs constitutively recruit B and T cells from the circulation (de Chaisemartin et al., 2011; Neyt et al., 2012). We noted prominent, large $CD31^+PNAd^+$ HEV-like structures, in many of which T cells in the lumen were associated with the vessel wall (Figures 3E–3V and Movie S2C). This indicates that HEV-like structures could be recruiting circulating T cells into TA-TLSs in this model, as has been hypothesized in humans. Together, these data demonstrate that TLSs associated with LucOS-expressing lung adenocarcinomas have hallmarks of LNs and phenotypically mirror TA-TLSs seen in cancer patients.

TLSs Facilitate T Cell Entry into and Activation in the Tumor Microenvironment

It has been speculated that TA-TLSs might be a site for local activation of tumor-specific T cells (Goc et al., 2013), but this possibility remains untested. Therefore, we focused on examining the function of TA-TLSs in vivo. Because LucOS/Cre LV encodes the antigenic portions of ova, we used ova-specific T cell receptor (TCR) transgenic (Tg) OT-I $CD45.1^+CD8^+$ T cells to analyze homing to and antigen presentation in TA-TLSs (outlined in Figure 4A). As a negative control, LCMV-specific P14 Tg $CD45.1^+CD8^+$ T cells were used because their TCR recognizes an antigen not present in LucOS. We activated the OT-I and P14 T cells in vitro to generate memory T cells, which are more sensitive for the presence of antigens (Kaech and Ahmed, 2001). Next, the OT-I and P14 T cells were labeled with the cell-proliferation dyes cell trace violet (CT-V) and eFluor670 (CT-670), respectively, mixed at a 1:1 ratio, and adoptively transferred into week-20 tumor-bearing $CD45.2^+$ KP-F mice or control

(A) FACS plots show lung $CD4^+$ T cells and are gated as in Figure 1A. n > 6 mice.
(B) Confocal IF images show the range (no or low, moderate, or severe) of tumor destruction in untreated (left panel) and Treg-cell-depleted (right three panels) mice. Red, $tdTomato^+$; green, EpCAM; blue, DAPI; dashed line, tumor border.
(C) Quantitation of tumor destruction from images in (C). n = 85 and 13 control tumors and mice, respectively, and 108 and 17 Treg-cell-depleted tumors and mice, respectively.
(D) Control (left panels) and Treg-cell-depleted (right panels) lungs were optically cleared with CLARITY. Images show optical slices through tumors. Red, $tdTomato^+$; green, YO-PRO-1. n = 15 and 7 control tumors and mice, respectively, and 10 and 3 Treg-cell-depleted tumors and mice, respectively. See also Movie S1.
(E) IHC images show control and Treg-cell-depleted tumors for lung (NKX2.1, brown) and immune (CD45, pink) cells. n = 71 and 11 control tumors and mice, respectively, and 55 and 9 Treg-cell-depleted tumors and mice, respectively.
(F) Graph of median lung-tissue $CD4^+$ and $CD8^+$ ($Thy1.2^+$) T cell and ($B220^+$ $CD19^+$) B cell numbers in Treg-cell-depleted mice (black bars, n = 6) and control mice (white bars, n = 5) ± SEM. *p = 0.0150, **p = 0.0175.
(G) Confocal IF images show control (n = 39) and Treg-cell-depleted (n = 15) tumors. Red, $tdTomato^+$; green, CD4; blue, $CD8^+$ T cells.
(H) Confocal IF image shows a Treg-cell-depleted tumor. Red, $tdTomato^+$; green, $CD11c^+$ macrophage (large round cells). The inset shows an optical slice of a macrophage with tdT^+ vesicles (the z depth is different than in the larger image). n = 4 mice.

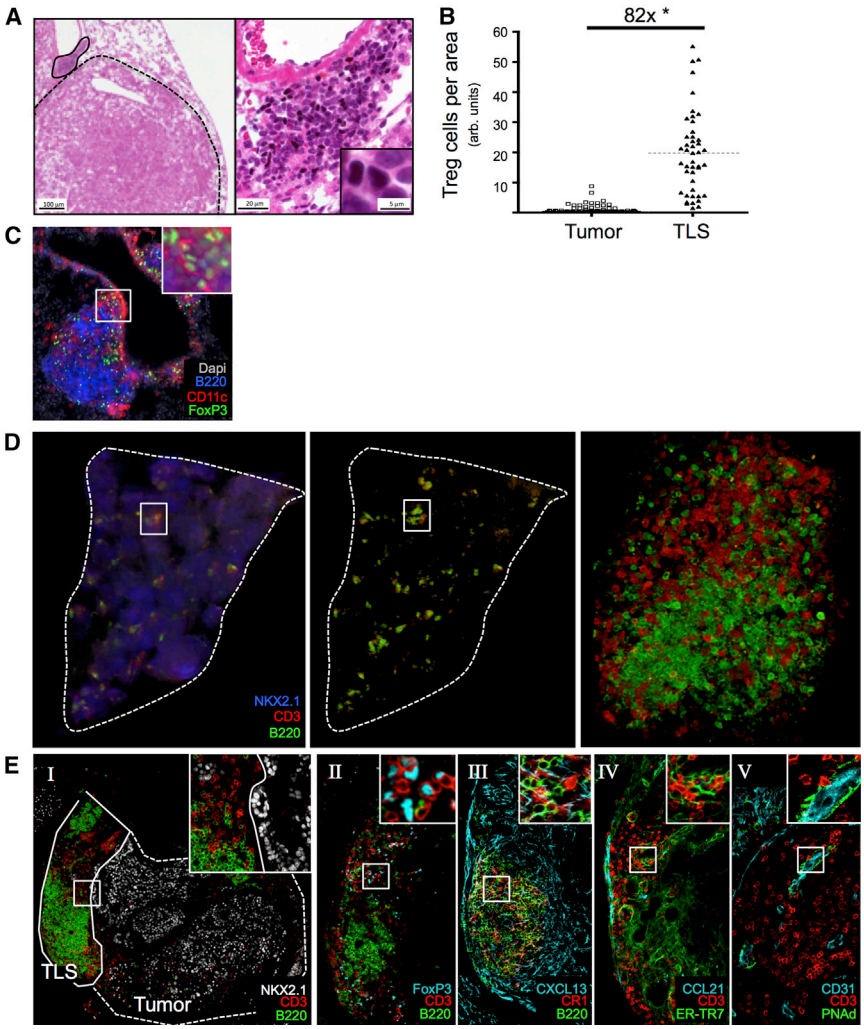

Figure 3. Treg Cells in Tumor-Bearing Lungs Are Located in TA-TLSs

KP-F or KPT-F mice were analyzed 18–20 weeks after LucOS/Cre LV infection.

(A) IHC images show FoxP3 (black), hematoxylin (blue), and eosin (pink). Tumor, dashed line; TLS, solid line; left panel, 4×; right panel, 20×. n = 10 mice.

(B) Median Treg cell number in tumors (n = 88) and TLSs (n = 45) from 9 mice. Normalized by pixel area. *$p = 3.89 \times 10^{-25}$.

(C) IF image shows TLSs. Red, CD11c; green, FoxP3; blue, B220; white, DAPI. n = 6 mice.

(D) 3D rendering of an in-silico-reconstructed tumor-bearing lung lobe. ~20 IF sections (50 μM, ~1-mm depth) were imaged by confocal microscopy. Blue, NKX2.1; red, CD3; green, B220. Center panel is the same as the left, except that NXK2.1 was removed. Right panel, TLS in box. n = 3 mice.

(E) Confocal IF images show a TLS in serial stained sections (30 μm) stained for indicated markers. The tumor border (dotted line) and TLS (solid line) are shown in (I). Images highlight (II) cyan $FoxP3^+$ Treg cells, (III) red $CR1^+$ FDCs, (IV) green ER-$TR7^+$ FRCs, and (V) green $PNAd^+CD31^+$ HEVs. n = 16 mice.

non-tumor-bearing $CD45.2^+$ P-F mice. On days 2 and 3 after transfer, homing, proliferation, and activation status were assessed by FACS and IF. When OT-I and P14 T cells were transferred to control mice, neither cell type appreciably entered the lung tissue, consistent with a lack of TLSs in these mice (Figure 4B). In contrast, upon transfer into tumor-bearing hosts, both OT-I and P14 T cells entered the lung tissue. This suggests that like LNs, TLSs in this model have the capacity to recruit activated T cells from the circulation. Both P14 and OT-I T cells were found in the lung tissue, but by IF a greater fraction of the OT-I T cells were located in the TLS (Figure 4C and Figure S5A). Furthermore, OT-I T cells were observed to interact with DCs in the T cell areas of the TLSs (Figure 4D). To determine whether these contacts were functionally relevant, we assessed whether OT-I and P14 T cells form immunologic synapses in vivo with DCs. Sections were stained with γ-tubulin (a marker of the microtubule-organizing center [MTOC]) and CD11c, and immunologic synapses were quantified on the basis of MTOC position and interaction with a DC (Figure S5B). In cells forming synapses, the MTOC is repositioned to lie behind the synapse and, as such, can be used for determining the direction in which a T cell is oriented (Billadeau et al., 2007). According to this metric, along with the accumulation of cell-proliferation dye (which non-specifically labels cellular protein) at the T-cell-DC interface, OT-I T cells formed 2.7-fold more synapses than did P14 T cells in TLSs (Figure 4E). A similar increase was seen among OT-I T cells transferred into LucOS/Cre-LV-infected versus Cre-LV-infected recipients, which have tumors that do not express LucOS (data not shown). Therefore, although OT-I and P14 T cells were both recruited into tumor-bearing lungs, OT-I T cells preferentially interacted with DCs in TLSs. This interaction had a meaningful effect on the OT-I T cells, such that they upregulated CD69, an early marker of T cell activation, and proliferated within lung tissue, whereas P14 T cells did not (Figure 4F). Similar activation and proliferation patterns were seen in the tumor-draining mLN, but not in the iLNs, spleen, or lung circulation (Figure 4F and data not shown). OT-I T cells did not upregulate CD69 or proliferate in the lung tissue or mLN when transferred into control P-F mice (data not shown). These data clearly demonstrate that infiltrating T cells can interact with tumor antigens in both the mLN and the TA-TLSs.

Because some DCs in the TLSs could have been directly infected by LucOS/Cre LV (20 weeks prior), and thus their presentation of antigens might not be tumor specific, we analyzed DCs in KPT-F mice for the presence of tdT by IF. Given that the highly active and ubiquitously expressed CAG promoter drives tdT expression after Cre-mediated recombination in KPT-F mice (Madisen et al., 2010), direct infection of any cell type results in strong tdT signal. 20 weeks after LucOS/Cre LV infection, directly infected round $CD11c^+$ macrophages were easily

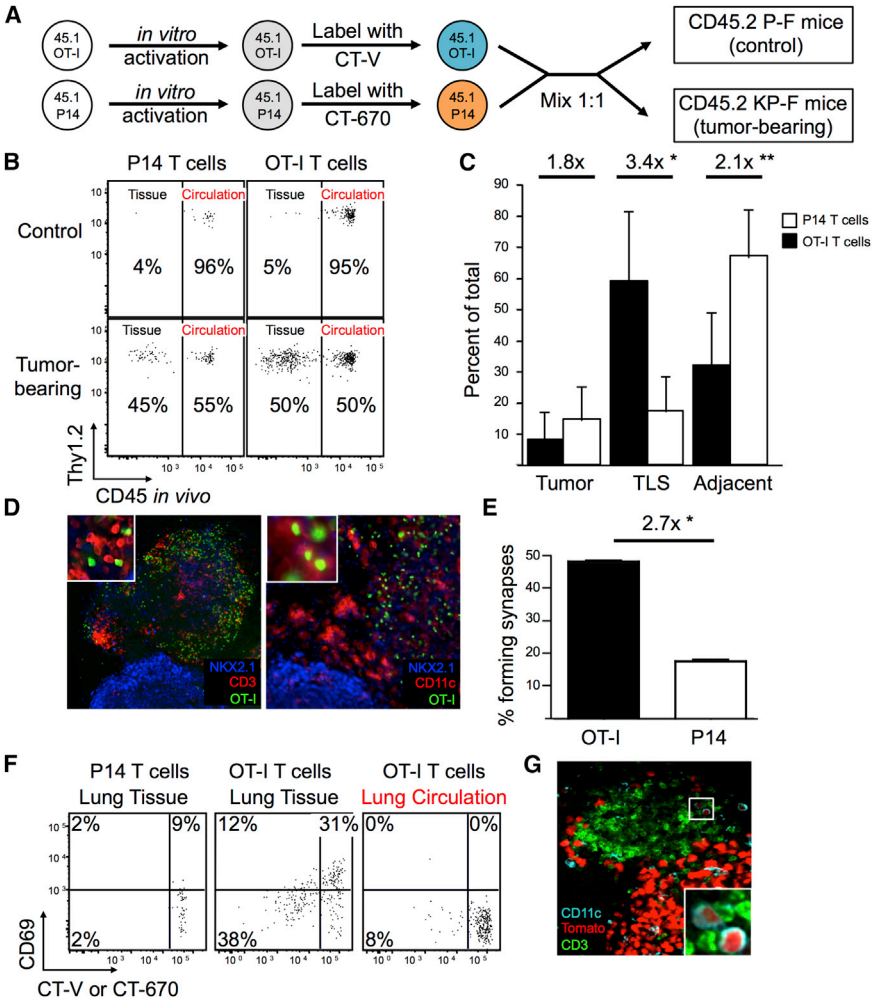

Figure 4. TLSs Serve as Local Sites of Tumor Antigen Presentation

(A) Schematic diagram for (B)–(F). In-vitro-activated CT-670$^+$ P14 and CT-V$^+$ OT-I Tg CD45.1$^+$CD8$^+$ T cells were transferred into ~week-20 LucOS/Cre-LV-infected CD45.2$^+$ tumor-bearing KP-F and control P-F recipients.

(B) FACS plots show lung CD45.1$^+$CD8$^+$ P14 and OT-I T cells 2–3 days after transfer. n > 12 mice per group.

(C) Graph shows the median fraction (± SEM) of transferred OT-I (black bars, n = 620) or P14 (white bars, n = 238) CD8$^+$ T cells in the indicated tissue (see also Figure S5A). *p = 1.89 × 10^{-3}, **p = 3.59 × 10^{-3}.

(D) Confocal IF images of a TLS. Green, CT-V (OT-I T cells); blue, NKX2.1; red, CD3 (left panel, n = 13) or CD11c (right panel, n > 20).

(E) Graph shows the mean fraction (± SEM) of OT-I (black bar, n = 231) or P14 (white bar, n = 122) T cells forming synapses (see also Figure S5B). *p = 5.62 × 10^{-11}.

(F) FACS plots show transferred P14 or OT-I CD8$^+$ T cells (gated as in Figure 5B). n > 12 recipients.

(G) Confocal IF image shows a tumor and TLS in ~week-20 LucOS/Cre-LV-infected KPT-F mice. Green, CD3; cyan, CD11c (DCs are small cells); red, tdTomato. Note the signal-intensity difference between tumor cells and DCs. n = 5 mice.

identified on the basis of an abundant tdT signal, similar in intensity to that in tumor cells (data not shown). In contrast, some CD11c$^+$ DCs (distinguished from macrophages on the basis of their smaller size and dendritic morphology; Thornton et al., 2012) had faint signal for tdT in TA-TLSs in KPT-F mice, implying that these cells had phagocytosed tumor-derived products (Figure 4G). Additionally, we sorted lung-tissue DCs from tumor-bearing lungs and confirmed that they could present tumor-derived antigens to naive OT-I CD8$^+$ T cells in vitro (Figures S5C and S5D). Together, these data demonstrate that much like the tumor-draining LNs, TA-TLSs in this tumor model are functional structures capable of recruiting circulating CD8$^+$ T cells and facilitating their interactions with antigen-presenting DCs.

Local Immune Responses in TA-TLSs after Treg Cell Depletion

We next assessed the impact of Treg cell depletion on tumor-associated TLSs. The area of the lung covered by TLSs from ~week-20 LucOS/Cre-LV-infected KP-F mice expanded ~7-fold in the 12 days after Treg cell depletion (Figure 5A). However, because it was unclear whether this increase was due to local lymphocyte expansion or recruitment, we analyzed TA-TLSs for signs of immune activity at early time points after Treg cell depletion. Antigen-driven lymphocyte activation is strongly correlated with cell division; therefore, we treated mice with the nucleoside analog bromodeoxyuridine (BrdU) 4 hr before sacrifice to label proliferation of lymphocytes. IHC analysis showed that the proportion of proliferating lymphocytes in TLSs was increased at days 4 and 6 after Treg cell depletion (Figures 5B and S6A). Moreover, analysis of BrdU incorporation by FACS and IF revealed that the increased rates of proliferation were largely among CD4$^+$ and CD8$^+$ T cells in TLSs, which increased ~5- and ~10-fold, respectively, after Treg cell depletion (Figures 5C and 5D). Collectively, these data suggest that TA-TLSs are local sites for T cell proliferation shortly after Treg cell depletion, although it is possible that some T cells proliferated elsewhere and migrated to TA-TLSs during the 4-hr window of our assay.

Treg cells directly regulate costimulatory molecules on DCs in SLOs (Kim et al., 2007), and we therefore reasoned that increased expression of costimulatory molecules on DCs immediately after Treg cell depletion could indicate sites of Treg cell function. Expression of CD80 (B7-1) and CD86 (B7-2) was examined on lung-tissue DCs 2 days after Treg cell depletion, when changes would most likely be due to direct effects in TLSs. FACS analysis of day-2 and day-6 Treg-cell-depleted mice revealed that lung-tissue DCs had higher expression of CD80 and CD86 at day 2 after depletion (Figure 5E). These data are consistent with the possibility that, as they do in other SLOs, Treg cells in TA-TLSs regulate DC

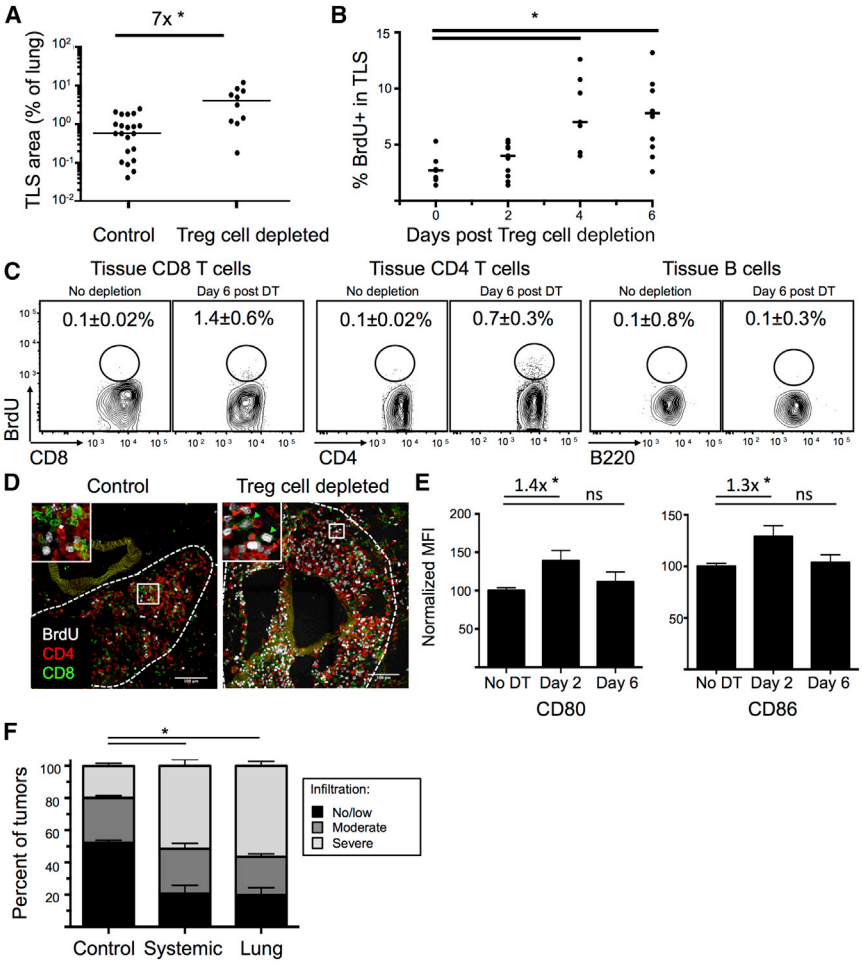

Figure 5. TLSs Are Sites of Immune Activation after Treg Cell Depletion

~week-20 LucOS/Cre-LV-infected KP-F mice received i.p. (A–F) or i.t. (F) DT injection. Mice were treated with BrdU for labeling proliferating cells (B–D).

(A) Graph quantifies TLS area (normalized to lung area) in 22 control and 10 day-12 Treg-cell-depleted mice. *p = 1.8 × 10^{-4}.

(B) Graph shows the percent of BrdU$^+$ lymphocytes in TLSs after Treg cell depletion. Day 0 indicates no DT. Points are the average of lymphocytes in all the TLSs in a section. Bars indicate the median. n = 7 (days 0 and 4) and 11 (days 2 and 6). *p < 0.005. See also Figure S6A.

(C) FACS plots show BrdU staining in lung-tissue CD8$^+$ and CD4$^+$ (FoxP3$^-$) T cells and B220$^+$CD19$^+$ B cells. Data represent the average ± SEM of three control and six Treg-cell-depleted mice.

(D) Confocal IF images show control (n = 18 TLSs and 9 mice) and day-6 Treg-cell-depleted (n = 57 TSLs and 12 mice) TLSs. Green, CD8; red, CD4; white, BrdU; arrowheads, BrdU$^+$CD8$^+$ (green) and CD4$^+$ (red) T cells.

(E) Graphs show median (± SEM) CD80 and CD86 median fluorescence intensity on lung-tissue CD11b$^+$CD11c$^+$MHCII$^+$ DCs. n = 8 (no DT), 12 (day 2), 13 (day 6). Relative change is indicated. ns, non-significant; *p < 0.05.

(F) Graph shows blind quantification of IHC on lung sections from control mice (n = 630 tumors and 23 mice), day-12 i.p.-DT-treated mice (systemic depletion, n = 136 tumors and 15 mice), and day-12 i.t.-DT-treated mice (lung-restricted depletion, n = 266 tumors and 11 mice) stained for CD45 and NKX2.1. No or low, <30% CD45$^+$ cell infiltration; moderate, 30%–50%; severe, >50%. *p < 0.005.

function by reducing costimulatory levels. Furthermore, after Treg cell depletion, the overall microenvironment in the TA-TLSs might become more immunostimulatory to promote anti-tumor responses by T cells.

Local Treg Cell Depletion Triggers Anti-tumor Responses Targeting Established Lung Adenocarcinomas

Treating tumor-bearing KP-F mice with i.p. DT causes acute systemic Treg cell depletion throughout the mice. To verify that Treg cells in the local microenvironment of the lung suppress anti-tumor responses, we treated mice with repeated low doses of i.t. DT to deplete Treg cells locally within the lung. Week-20 LucOS/Cre-LV-infected KP-F mice were treated with six daily i.t. doses of 50 ng DT. Administering i.t. DT did not result in LN enlargement, with the exception of the lung-draining mLN, and no morbidity was observed (data not shown). Local Treg cell depletion triggered immune infiltration of ~80% of lung tumors (Figures 5F and S6B). Therefore, local Treg cell depletion was sufficient to trigger strong anti-tumor effects, consistent with the idea that Treg cells in the TLSs (and possibly in the mLNs) regulate local anti-tumor responses. Moreover, these data demonstrate that efficient, local Treg cell depletion could be an effective means of triggering endogenous anti-tumor immune responses without the systemic toxicity associated with whole-body Treg cell depletion.

Programmed Antigen Expression Is Not Required for Anti-tumor Responses after Treg Cell Depletion

We next examined whether Treg cell depletion enhanced responses by the CD8$^+$ T cells targeting the potent T cell antigens in LucOS. Surprisingly, however, we found that the number of endogenous SIINFEKL-specific CD8$^+$ T cells (identified with SIINFEKL-loaded H2-K^b MHC I tetramers) was not dramatically altered by Treg cell depletion (Figures 6A). Additionally, the responses of naive T cell OT-I CD8$^+$ T cells transferred into tumor-bearing recipients were not enhanced by the absence of Treg cells (data not shown). These data suggest that programmed antigen expression by tumors is not required to elicit anti-tumor responses after Treg cell depletion. Thus, we infected KP-F and KP × *FoxP3*$^{IRES\text{-}RFP}$ (KP-RFP) mice with Cre LV (previously referred to as Lenti-X in DuPage et al., 2011), and ~18 weeks later, we treated them with DT. After 12 days, we analyzed lung tumors for infiltration by immune cells and evidence of tumor destruction. Treg cell depletion resulted in dramatic infiltration of lung tissues by CD45$^+$ cells, particularly in the perivascular and peribronchiolar regions (data not shown). Moreover, ~75% of tumors in Treg-cell-depleted mice (n = 174

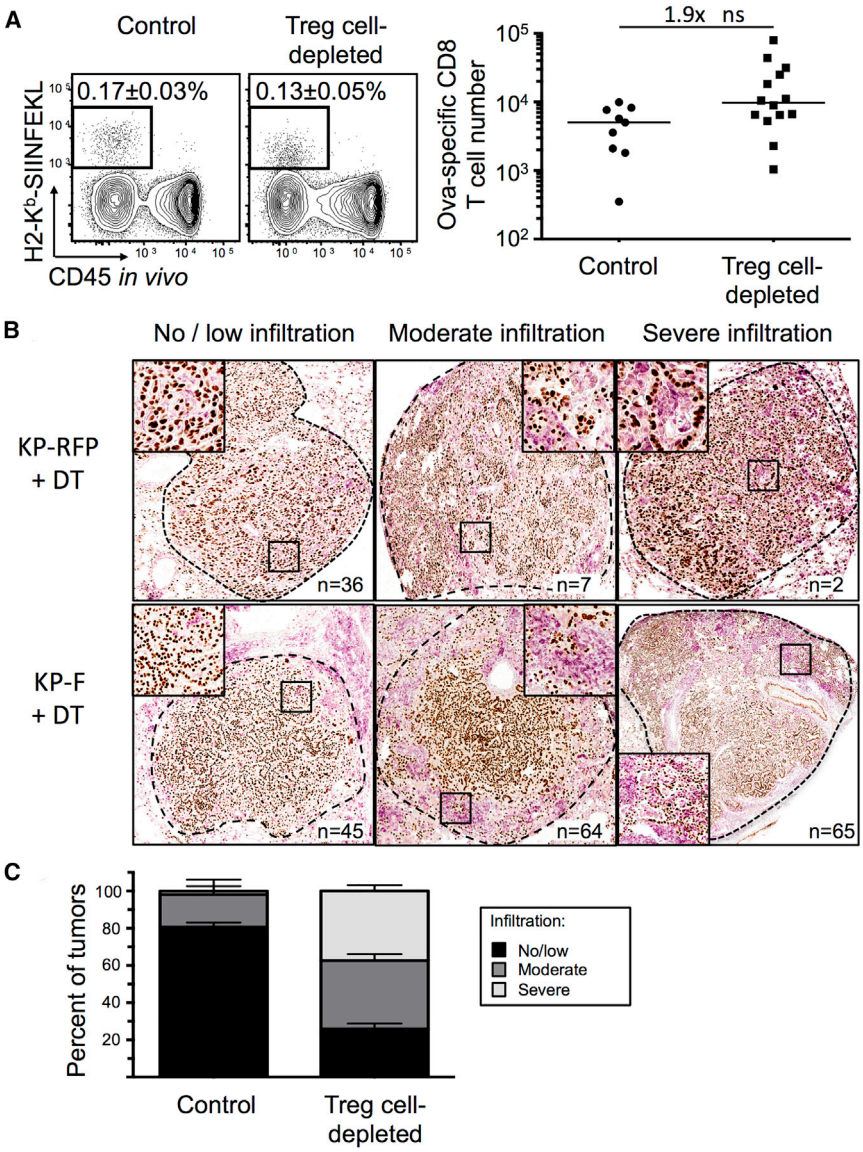

Figure 6. Overt Antigen Expression by Tumors Is Not Required for Anti-tumor Response after Treg Cell Depletion

(A) FACS plots and graph show endogenous ova-specific CD8$^+$ T cells (identified with H2-K^b-SIINFEKL tetramer) in control (n = 9) and day-12 Treg-cell-depleted (i.p.; n = 14) ~week-20 LucOS/Cre-LV-infected KP-F mice. Plots are gated on CD8$^+$ T cells. Median frequency of total ± SEM is indicated on plots. Note that no tetramer staining was observed in Cre-LV-infected mice. ns, non-significant.

(B) IHC images show NKX2.1 (brown) and CD45 (pink) in ~week-18 Cre-LV-infected KP-F (n = 15) and KP-RFP (control, n = 6) mice 12 days after i.p. DT injection. No or low, <30% CD45$^+$ cell infiltration; moderate, 30%–50%; severe, >50%. n = tumor number.

(C) Graph quantifies IHC in (B). Control includes tumors from DT-treated KP-RFP mice (n = 45 tumors and 6 mice) and untreated KP-F mice (n = 58 tumors and 5 mice). n = 174 Treg-cell-depleted tumors from 10 mice.

tumors from 10 mice) were moderately (immune infiltration in 30%–50% of the tumor area) or severely (greater than 50%) infiltrated, and most showed evidence of immune-mediated tumor disruption (Figures 6B and 6C). In contrast, ~20% of the tumors from DT-treated KP-RFP mice (n = 45 tumors from 6 mice) had moderate or severe immune infiltration (Figures 6B and 6C). Similarly, only 10% of non-DT-treated week-20 KP-F mice (n = 58 tumors from 5 mice) had severe or moderate infiltration. These data clearly demonstrate that the anti-tumor response seen after Treg cell depletion does not require the programmed expression of strong tumor antigens by tumors.

DISCUSSION

It is thought that the intratumoral Treg cells in cancer patients have important roles in immunosuppression, but it has not been possible to functionally explore these roles in humans. Here, we have demonstrated that Treg cells regulate anti-tumor immune responses in TA-TLSs in a mouse model of lung adenocarcinoma. We observed that TLSs recruit T cells from the circulation and facilitate their interaction with tumor-antigen-presenting DCs. Treg cells in TLSs actively suppress potent anti-tumor responses, and thus TLSs are a primary site for T cell expansion upon Treg cell depletion. Subsequently, T cells and macrophages infiltrate tumors, resulting in significant tumor destruction. Collectively, these data point to immunosuppressive Treg cell function within TLSs as one mechanism that prevents anti-tumor responses and allows continued tumor development.

TA-TLSs have been observed in several human cancer types (Fridman et al., 2012; Goc et al., 2013), but it is not known how they form or function. In this model, TA-TLSs formed during the course of tumor development and were closely associated with ~90% of the LucOS-expressing tumors. Interestingly, antigen expression by tumors might affect TLS formation given that TLSs in lungs from Cre-LV-infected mice appeared larger and were located centrally in the lungs, distal to tumors (N.S.J. and T.J., unpublished data).

In most studies, the presence of TA-TLSs correlates with better survival for cancer patients, suggesting that TA-TLSs have anti-tumor functions. However, one study found that high numbers of Treg cells in TA-TLSs, but not the tumor parenchyma, correlated with poor survival of breast cancer patients (Gobert et al., 2009). It has been difficult to study the function of TA-TLSs, including how immunosuppressive pathways, like Treg cells, influence anti-tumor responses from within these structures. In this model, we observed that Treg cells were prominent in TA-TLSs and that, upon Treg cell depletion, T cells within TA-TLSs proliferated, coincident with tumor infiltration. Thus, we

propose that TA-TLSs might serve both pro- and anti-tumor functions depending on the state of disease progression, as well as the presence of immunosuppressive cell types, including Treg cells. However, TA-TLSs also probably facilitate influx of new effector T cells into the tumor site after Treg cell depletion through HEVs and amplify the anti-tumor response. Therefore, TA-TLSs could be intimately involved in many aspects of the anti-tumor immune response, both at steady state and after therapeutic interventions.

The data presented here do not exclude the possibility that Treg cells in this model also suppress anti-tumor responses in the tumor-draining mLN. In contrast, because tumor antigens are presented in TA-TLSs and the mLN, regulation of anti-tumor immune responses most likely requires immunosuppression at both sites. Because Treg cells function through a variety of mechanisms (Josefowicz et al., 2012), Treg cells in TA-TLSs and LNs could rely on distinct effector pathways. Consistent with this idea, Treg cells in TA-TLSs were phenotypically more activated and expressed higher levels of multiple effector molecules. For example, Treg cells in our model (and others) expressed higher amounts of CTLA-4 in the tumor microenvironment than did tumor-draining LNs (Marabelle et al., 2013; McDermott et al., 2014; Selby et al., 2013; Simpson et al., 2013). In the steady state, Treg cells use CTLA-4 to reduce the amounts of costimulatory proteins on DCs, thus inhibiting T cell activation and preventing autoimmunity (Qureshi et al., 2011; Wing et al., 2008). Likewise, Treg cells in TLSs could use CTLA-4 to regulate anti-tumor responses through DCs. TA-TLS Treg cells also express high amounts of CD39, which, along with CD73, produces adenosine, a potent T cell inhibitor (Antonioli et al., 2013). Interestingly, chemical inhibition of CD39 has been shown to reduce early tumor growth in a Kras-driven *Atg5*-deficient mouse lung cancer model, possibly through Treg cell function (Rao et al., 2014). Further investigation will be required to more firmly establish the functional importance of these and other effector pathways active in Treg cells in TLSs and to determine whether these pathways can be therapeutically exploited for improving anti-tumor immune responses.

$CD8^+$ T cell responses against the strong ova-antigen in LucOS were not dramatically enhanced by Treg cell depletion. This is perhaps because Treg cells preferentially suppress responses by T cells that have weak, lower-affinity interactions with their cognate antigen (Pace et al., 2012), more like those seen with self- or tumor-antigens (Aleksic et al., 2012). Therefore, in addition to responding to Cre-derived antigens, after Treg cell depletion, T cells could also have been responding to self-antigens expressed by tumors in this model. Overexpressed and abnormally expressed (non-mutated) antigens are frequent targets in human cancer (Finn, 2008), and advanced lung tumors in KP mice can express embryonic proteins and proteins normally found in other locations, such as the gut (Snyder et al., 2013). Responses against these antigens would be suppressed under steady-state conditions, but it is possible that Treg cell depletion permits responses by T cells with low affinity for these tumor-associated antigens. Identification of the types of tumor antigens recognized by T cells after Treg cell depletion will be helpful for guiding the development of future immune-based therapies.

Immune-checkpoint blockers have enormous potential for treating a variety of types of human cancers, but positive clinical responses correlate with immune-related adverse events (Pardoll, 2012). Because immune-checkpoint pathways are important for preventing naturally occurring autoimmune diseases, immunotherapies walk a fine line between promoting strong anti-cancer effects and minimizing autoimmune toxicity. Treg cells are prime immunotherapeutic targets. In our model, systemic Treg cell depletion unleashed a powerful anti-tumor response but also resulted in significant morbidity. Therefore, it seems possible that it could be difficult to control the autoimmune response triggered by systemic Treg cell depletion in patients once it is initiated. This concern underscores the need to identify mechanisms for localized therapeutic depletion or targeted blockade of Treg cells in the tumor microenvironment. For example, some CTLA-4 antibodies can deplete intratumoral Treg cells, and treatment of metastatic melanoma patients with a Treg-cell-depleting antibody, ipilimumab, provides an increase in overall survival, whereas treatment with a non-depleting antibody, tremelimumab, does not (Hodi et al., 2010; Ribas et al., 2013; Marabelle et al., 2013; McDermott et al., 2014; Selby et al., 2013; Simpson et al., 2013). From a therapeutic standpoint, specifically targeting immunosuppressive mediators in TA-TLSs (like Treg cells) could make it possible to promote local anti-tumor responses and maintain immune homeostasis outside of the tumor microenvironment. Our study supports the development of additional targets for local Treg cell inhibition within the tumor microenvironment as a strategy that could provide safer, more-effective therapy for patients with cancer.

EXPERIMENTAL PROCEDURES

Mice and Treatments

KP and *Foxp3*$^{IRES\text{-}DTR\text{-}GFP}$ mice have been previously described (DuPage et al., 2011; Kim et al., 2007). OT-I TCR Tg and *Rosa26*$^{LSL\text{-}tdT}$ mice (B6.Cg-Gt(ROSA)26Sor$^{tm14(CAG\text{-}tdTomato)Hze/J}$) were purchased from the Jackson Laboratory, and P14 TCR Tg mice were purchased from Taconic. For systemic Treg cell depletion, mice received i.p. injection of 50 ng/g DT in PBS on days 0 and 1 (two doses). For lung-specific Treg cell depletion, mice received i.t. injection of 50 ng DT in 50–100 μl PBS on days 0–5 (six doses). Mice tolerated i.t. DT well, and no morbidity or mortality was observed. Furthermore, i.t. DT did not trigger splenomegaly or lymphadenopathy, except in the lung-draining mediastinal LNs (data not shown). Details of BrdU labeling, in vivo labeling, and MRI are provided in the Supplemental Experimental Procedures. All studies were performed under an animal protocol approved by the Massachusetts Institute of Technology (MIT) Committee on Animal Care. Mice were assessed for morbidity according to guidelines set by the MIT Division of Comparative Medicine and were always humanely sacrificed prior to natural expiration.

Lentiviral Production

Mice received i.t. injection of 2.5×10^4 to 5×10^4 PFU of Cre or LucOS/Cre LV for tumor initiation. Details of the viruses and production are provided in the Supplemental Experimental Procedures.

Tissue Isolation, Immunohistochemistry, and Immunofluorescence

Lungs were isolated, flushed with bronchoalveolar lavage and/or lung circulatory perfusion, and then allocated for IHC, IF, FACS, and/or CLARITY. For IHC and IF, tissues were preserved overnight with paraformaldehyde-lysine-periodate fixative, embedded in paraffin (IHC) or cryoprotected with 30% sucrose in PBS (IF), and embedded in optimum cutting temperature compound (VWR). Details of isolation, fixation, and IF and IHC staining are provided in the Supplemental Experimental Procedures.

Confocal Imaging

Images were acquired on an Olympus FV1200 Laser Scanning Confocal Microscope or a Nikon A1R Ultra-Fast Spectral Scanning Confocal Microscope with 10×, 20×, and 30× objectives and analyzed with ImageJ (NIH) and Photoshop CS4 (Adobe Systems). For whole-lung reconstructions, individual sections were manually aligned with ImageJ and Photoshop as detailed in the Supplemental Experimental Procedures.

Flow Cytometry

Spleens and LNs were processed as described in Joshi et al. (2007). Lungs were prepared with a gentleMACS dissociator and C tubes (Miltenyi Biotec) as described in the Supplemental Experimental Procedures. Samples were analyzed with an LSR II (BD) and FlowJo software (Tree Star). Cell sorting was performed on a FACSAria III (BD).

Statistical Analyses and Quantifications

p values from unpaired two-tailed Student's t tests were used for all statistical comparisons. Tumor destruction based on the disruption of tumor morphology and infiltration by $CD45^+$ immune cells was scored as described in the Supplemental Experimental Procedures.

In Vitro T Cell Activation and Adoptive Transfer

Splenocytes from OT-I or P14 TCR Tg mice were stimulated in vitro, stained with cell-proliferation dyes, and mixed at a 1:1 ratio as detailed in the Supplemental Experimental Procedures. 1×10^6 to 5×10^6 cells were then transferred intravenously into ~week-20 LucOS/Cre-LV-infected recipient 45.2 KP-F mice.

Quantifying the Percentage of $BrdU^+$ from IHC Sections

Sections of lungs were stained for BrdU by IHC, counterstained, and imaged with an Aperio slide scanner (Leica). TA-TLSs (distinct clusters of lymphocytes associated with blood vessels) were cropped with Adobe Photoshop. Cropped images were quantified by CellProfiler for nuclei and $BrdU^+$ cells for determining the fraction of proliferating lymphocytes.

SUPPLEMENTAL INFORMATION

Supplemental Information includes six figures, Supplemental Experimental Procedures, and two movies and can be found with this article online at http://dx.doi.org/10.1016/j.immuni.2015.08.006.

AUTHOR CONTRIBUTIONS

N.S.J. and T.J. designed the study, and N.S.J. wrote the manuscript. N.S.J., E.H.A.-G., Y.L., D.-Y.L., G.P.C., A.L., R.R., D.M.C., and A.F.F. generated primary data. M.D. initiated the project. T.T. and N.R.K. established the CLARITY method in the laboratory. R.T.B. graded tumors. T.J. supervised data analysis and experiments.

ACKNOWLEDGMENTS

We thank Professor Alexander Rudensky (Memorial Sloan-Kettering Cancer Center) for the generous gift of *Foxp3*$^{DTR\text{-}GFP}$ mice and T.J. lab members for reviewing the manuscript. We also thank the Swanson Biotechnology Center: Kathleen Cormier in the Hope Babette Tang (1983) Histology Facility, Eliza Vasile and Jeff Wyckoff in the Microscopy Facility, Scott Malstrom in the Animal Imaging & Preclinical Testing Core Facility, Glenn Paradis in the Flow Cytometry Facility, and the KI Media Facility. This work was supported by NCI Cancer Center Support Grant P30-CA14051 and grants from the Howard Hughes Medical Institute (T.J.); NIH grants 1 U54 CA126515-01 (T.J.), R01-CA185020-01 (T.J.), and T32 GM007753 (A.L.); the Damon Runyon Cancer Foundation (N.S.J.); the Margaret A. Cunningham Immune Mechanisms in Cancer Research Fellowship Award (N.S.J.); and the Lung Cancer Research Foundation (N.S.J.). T.J. is a Howard Hughes Medical Institute Investigator and a Daniel K. Ludwig Scholar. This paper is dedicated to Professor Herman Eisen and to Officer Sean Collier for his caring service to the MIT community and for his sacrifice.

Received: June 2, 2015
Revised: June 2, 2015
Accepted: June 19, 2015
Published: September 1, 2015

REFERENCES

Aleksic, M., Liddy, N., Molloy, P.E., Pumphrey, N., Vuidepot, A., Chang, K.M., and Jakobsen, B.K. (2012). Different affinity windows for virus and cancer-specific T-cell receptors: implications for therapeutic strategies. Eur. J. Immunol. *42*, 3174–3179.

Antonioli, L., Pacher, P., Vizi, E.S., and Haskó, G. (2013). CD39 and CD73 in immunity and inflammation. Trends Mol. Med. *19*, 355–367.

Beyersdorf, N., Ding, X., Tietze, J.K., and Hanke, T. (2007). Characterization of mouse CD4 T cell subsets defined by expression of KLRG1. Eur. J. Immunol. *37*, 3445–3454.

Billadeau, D.D., Nolz, J.C., and Gomez, T.S. (2007). Regulation of T-cell activation by the cytoskeleton. Nat. Rev. Immunol. *7*, 131–143.

Boissonnas, A., Scholer-Dahirel, A., Simon-Blancal, V., Pace, L., Valet, F., Kissenpfennig, A., Sparwasser, T., Malissen, B., Fetler, L., and Amigorena, S. (2010). Foxp3+ T cells induce perforin-dependent dendritic cell death in tumor-draining lymph nodes. Immunity *32*, 266–278.

Bos, P.D., Plitas, G., Rudra, D., Lee, S.Y., and Rudensky, A.Y. (2013). Transient regulatory T cell ablation deters oncogene-driven breast cancer and enhances radiotherapy. J. Exp. Med. *210*, 2435–2466.

Campbell, D.J., and Koch, M.A. (2011). Phenotypical and functional specialization of FOXP3+ regulatory T cells. Nat. Rev. Immunol. *11*, 119–130.

Cheng, G., Yuan, X., Tsai, M.S., Podack, E.R., Yu, A., and Malek, T.R. (2012). IL-2 receptor signaling is essential for the development of Klrg1+ terminally differentiated T regulatory cells. J. Immunol. *189*, 1780–1791.

Chung, K., Wallace, J., Kim, S.Y., Kalyanasundaram, S., Andalman, A.S., Davidson, T.J., Mirzabekov, J.J., Zalocusky, K.A., Mattis, J., Denisin, A.K., et al. (2013). Structural and molecular interrogation of intact biological systems. Nature *497*, 332–337.

de Chaisemartin, L., Goc, J., Damotte, D., Validire, P., Magdeleinat, P., Alifano, M., Cremer, I., Fridman, W.H., Sautès-Fridman, C., and Dieu-Nosjean, M.C. (2011). Characterization of chemokines and adhesion molecules associated with T cell presence in tertiary lymphoid structures in human lung cancer. Cancer Res. *71*, 6391–6399.

Dieu-Nosjean, M.C., Antoine, M., Danel, C., Heudes, D., Wislez, M., Poulot, V., Rabbe, N., Laurans, L., Tartour, E., de Chaisemartin, L., et al. (2008). Long-term survival for patients with non-small-cell lung cancer with intratumoral lymphoid structures. J. Clin. Oncol. *26*, 4410–4417.

DuPage, M., and Jacks, T. (2013). Genetically engineered mouse models of cancer reveal new insights about the antitumor immune response. Curr. Opin. Immunol. *25*, 192–199.

DuPage, M., Cheung, A.F., Mazumdar, C., Winslow, M.M., Bronson, R., Schmidt, L.M., Crowley, D., Chen, J., and Jacks, T. (2011). Endogenous T cell responses to antigens expressed in lung adenocarcinomas delay malignant tumor progression. Cancer Cell *19*, 72–85.

DuPage, M., Mazumdar, C., Schmidt, L.M., Cheung, A.F., and Jacks, T. (2012). Expression of tumour-specific antigens underlies cancer immunoediting. Nature *482*, 405–409.

Feuerer, M., Hill, J.A., Kretschmer, K., von Boehmer, H., Mathis, D., and Benoist, C. (2010). Genomic definition of multiple ex vivo regulatory T cell subphenotypes. Proc. Natl. Acad. Sci. USA *107*, 5919–5924.

Finn, O.J. (2008). Cancer immunology. N. Engl. J. Med. *358*, 2704–2715.

Fridman, W.H., Pagès, F., Sautès-Fridman, C., and Galon, J. (2012). The immune contexture in human tumours: impact on clinical outcome. Nat. Rev. Cancer *12*, 298–306.

Gobert, M., Treilleux, I., Bendriss-Vermare, N., Bachelot, T., Goddard-Leon, S., Arfi, V., Biota, C., Doffin, A.C., Durand, I., Olive, D., et al. (2009). Regulatory T cells recruited through CCL22/CCR4 are selectively activated

in lymphoid infiltrates surrounding primary breast tumors and lead to an adverse clinical outcome. Cancer Res. *69*, 2000–2009.

Goc, J., Fridman, W.H., Sautès-Fridman, C., and Dieu-Nosjean, M.C. (2013). Characteristics of tertiary lymphoid structures in primary cancers. OncoImmunology *2*, e26836.

Hayes, S.A., Hudson, A.L., Clarke, S.J., Molloy, M.P., and Howell, V.M. (2014). From mice to men: GEMMs as trial patients for new NSCLC therapies. Semin. Cell Dev. Biol. *27*, 118–127.

Hodi, F.S., O'Day, S.J., McDermott, D.F., Weber, R.W., Sosman, J.A., Haanen, J.B., Gonzalez, R., Robert, C., Schadendorf, D., Hassel, J.C., et al. (2010). Improved survival with ipilimumab in patients with metastatic melanoma. N. Engl. J. Med. *363*, 711–723.

Jemal, A., Siegel, R., Xu, J., and Ward, E. (2010). Cancer statistics, 2010. CA Cancer J. Clin. *60*, 277–300.

Josefowicz, S.Z., Lu, L.F., and Rudensky, A.Y. (2012). Regulatory T cells: mechanisms of differentiation and function. Annu. Rev. Immunol. *30*, 531–564.

Joshi, N.S., Cui, W., Chandele, A., Lee, H.K., Urso, D.R., Hagman, J., Gapin, L., and Kaech, S.M. (2007). Inflammation directs memory precursor and short-lived effector CD8(+) T cell fates via the graded expression of T-bet transcription factor. Immunity *27*, 281–295.

Kaech, S.M., and Ahmed, R. (2001). Memory CD8+ T cell differentiation: initial antigen encounter triggers a developmental program in naïve cells. Nat. Immunol. *2*, 415–422.

Kim, J.M., Rasmussen, J.P., and Rudensky, A.Y. (2007). Regulatory T cells prevent catastrophic autoimmunity throughout the lifespan of mice. Nat. Immunol. *8*, 191–197.

Kwon, M.C., and Berns, A. (2013). Mouse models for lung cancer. Mol. Oncol. *7*, 165–177.

Lin, W., Truong, N., Grossman, W.J., Haribhai, D., Williams, C.B., Wang, J., Martín, M.G., and Chatila, T.A. (2005). Allergic dysregulation and hyperimmunoglobulinemia E in Foxp3 mutant mice. J. Allergy Clin. Immunol. *116*, 1106–1115.

Madisen, L., Zwingman, T.A., Sunkin, S.M., Oh, S.W., Zariwala, H.A., Gu, H., Ng, L.L., Palmiter, R.D., Hawrylycz, M.J., Jones, A.R., et al. (2010). A robust and high-throughput Cre reporting and characterization system for the whole mouse brain. Nat. Neurosci. *13*, 133–140.

Marabelle, A., Kohrt, H., Sagiv-Barfi, I., Ajami, B., Axtell, R.C., Zhou, G., Rajapaksa, R., Green, M.R., Torchia, J., Brody, J., et al. (2013). Depleting tumor-specific Tregs at a single site eradicates disseminated tumors. J. Clin. Invest. *123*, 2447–2463.

McDermott, D., Lebbé, C., Hodi, F.S., Maio, M., Weber, J.S., Wolchok, J.D., Thompson, J.A., and Balch, C.M. (2014). Durable benefit and the potential for long-term survival with immunotherapy in advanced melanoma. Cancer Treat. Rev. *40*, 1056–1064.

Neyt, K., Perros, F., GeurtsvanKessel, C.H., Hammad, H., and Lambrecht, B.N. (2012). Tertiary lymphoid organs in infection and autoimmunity. Trends Immunol. *33*, 297–305.

Pace, L., Tempez, A., Arnold-Schrauf, C., Lemaitre, F., Bousso, P., Fetler, L., Sparwasser, T., and Amigorena, S. (2012). Regulatory T cells increase the avidity of primary CD8+ T cell responses and promote memory. Science *338*, 532–536.

Pardoll, D.M. (2012). The blockade of immune checkpoints in cancer immunotherapy. Nat. Rev. Cancer *12*, 252–264.

Qureshi, O.S., Zheng, Y., Nakamura, K., Attridge, K., Manzotti, C., Schmidt, E.M., Baker, J., Jeffery, L.E., Kaur, S., Briggs, Z., et al. (2011). Trans-endocytosis of CD80 and CD86: a molecular basis for the cell-extrinsic function of CTLA-4. Science *332*, 600–603.

Raez, L.E., Fein, S., and Podack, E.R. (2005). Lung cancer immunotherapy. Clin. Med. Res. *3*, 221–228.

Rajasagi, M., Shukla, S.A., Fritsch, E.F., Keskin, D.B., DeLuca, D., Carmona, E., Zhang, W., Sougnez, C., Cibulskis, K., Sidney, J., et al. (2014). Systematic identification of personal tumor-specific neoantigens in chronic lymphocytic leukemia. Blood *124*, 453–462.

Rao, S., Tortola, L., Perlot, T., Wirnsberger, G., Novatchkova, M., Nitsch, R., Sykacek, P., Frank, L., Schramek, D., Komnenovic, V., et al. (2014). A dual role for autophagy in a murine model of lung cancer. Nat. Commun. *5*, 3056.

Ribas, A., Kefford, R., Marshall, M.A., Punt, C.J., Haanen, J.B., Marmol, M., Garbe, C., Gogas, H., Schachter, J., Linette, G., et al. (2013). Phase III randomized clinical trial comparing tremelimumab with standard-of-care chemotherapy in patients with advanced melanoma. J. Clin. Oncol. *31*, 616–622.

Robbins, S.H., Tessmer, M.S., Van Kaer, L., and Brossay, L. (2005). Direct effects of T-bet and MHC class I expression, but not STAT1, on peripheral NK cell maturation. Eur. J. Immunol. *35*, 757–765.

Sakaguchi, S. (2004). Naturally arising CD4+ regulatory t cells for immunologic self-tolerance and negative control of immune responses. Annu. Rev. Immunol. *22*, 531–562.

Sather, B.D., Treuting, P., Perdue, N., Miazgowicz, M., Fontenot, J.D., Rudensky, A.Y., and Campbell, D.J. (2007). Altering the distribution of Foxp3(+) regulatory T cells results in tissue-specific inflammatory disease. J. Exp. Med. *204*, 1335–1347.

Selby, M.J., Engelhardt, J.J., Quigley, M., Henning, K.A., Chen, T., Srinivasan, M., and Korman, A.J. (2013). Anti-CTLA-4 antibodies of IgG2a isotype enhance antitumor activity through reduction of intratumoral regulatory T cells. Cancer Immunol. Res. *1*, 32–42.

Simpson, T.R., Li, F., Montalvo-Ortiz, W., Sepulveda, M.A., Bergerhoff, K., Arce, F., Roddie, C., Henry, J.Y., Yagita, H., Wolchok, J.D., et al. (2013). Fc-dependent depletion of tumor-infiltrating regulatory T cells co-defines the efficacy of anti-CTLA-4 therapy against melanoma. J. Exp. Med. *210*, 1695–1710.

Snyder, E.L., Watanabe, H., Magendantz, M., Hoersch, S., Chen, T.A., Wang, D.G., Crowley, D., Whittaker, C.A., Meyerson, M., Kimura, S., and Jacks, T. (2013). Nkx2-1 represses a latent gastric differentiation program in lung adenocarcinoma. Mol. Cell *50*, 185–199.

Suffia, I., Reckling, S.K., Salay, G., and Belkaid, Y. (2005). A role for CD103 in the retention of CD4+CD25+ Treg and control of Leishmania major infection. J. Immunol. *174*, 5444–5455.

Teng, M.W., Ngiow, S.F., von Scheidt, B., McLaughlin, N., Sparwasser, T., and Smyth, M.J. (2010). Conditional regulatory T-cell depletion releases adaptive immunity preventing carcinogenesis and suppressing established tumor growth. Cancer Res. *70*, 7800–7809.

Thornton, E.E., Looney, M.R., Bose, O., Sen, D., Sheppard, D., Locksley, R., Huang, X., and Krummel, M.F. (2012). Spatiotemporally separated antigen uptake by alveolar dendritic cells and airway presentation to T cells in the lung. J. Exp. Med. *209*, 1183–1199.

Vogelstein, B., Papadopoulos, N., Velculescu, V.E., Zhou, S., Diaz, L.A., Jr., and Kinzler, K.W. (2013). Cancer genome landscapes. Science *339*, 1546–1558.

Wing, K., Onishi, Y., Prieto-Martin, P., Yamaguchi, T., Miyara, M., Fehervari, Z., Nomura, T., and Sakaguchi, S. (2008). CTLA-4 control over Foxp3+ regulatory T cell function. Science *322*, 271–275.